Nuclear Instruments and Methods in Physics Research A 351 (1994) 359–370

NUCLEAR INSTRUMENTS & METHODS IN PHYSICS RESEARCH Section A

The construction and operation of a hybrid gas–silicon detector for studies of cluster breakup reactions

Charissa Collaboration

N. Curtis [a], A. St.J. Murphy [a], M.J. Leddy [a,1], J.S. Pople [a], N.M. Clarke [a,*], M. Freer [a], B.R. Fulton [a], S.J. Hall [a], G. Tungate [a], R.P. Ward [a], S.M. Singer [b], W.N. Catford [b], G.J. Gyapong [b], R.A. Cunningham [c], J.S. Lilley [c,1], S.P. Chappell [d], S.P. Fox [d], C.D. Jones [d], D.L. Watson [d], P.M. Simmons [e], R.A. Hunt [e], A.C. Merchant [e], A.E. Smith [e,2], W.D.M. Rae [e], J. Zhang [e,3]

[a] *School of Physics and Space Research, University of Birmingham, Edgbaston, Birmingham, B15 2TT, UK*
[b] *Department of Physics, University of Surrey, Guildford, Surrey, GU2 5XH, UK*
[c] *Daresbury Laboratory, Warrington, WA4 4AD, UK*
[d] *Department of Physics, University of York, York YO1 5DD, UK*
[e] *Department of Nuclear Physics, University of Oxford, Oxford, OX1 3RH, UK*

Received 27 June 1994

Abstract

A hybrid detector system has been constructed consisting of a gas filled ionization chamber and a large area silicon semiconductor strip detector within the same gas volume. The construction and operation of these detectors is described, together with a brief description of the electronics and data acquisition system used in cluster breakup studies. The techniques for software correction and gain matching of the detector energy signals are described and results are presented for the resolutions in energy, position and time. In a typical application, elements up to Ca are easily resolved and the positions of individual ions are measured with a resolution of <0.2 mm in the reaction plane, whilst energy resolutions approaching 200 keV can be obtained from the Si strip detector over a small area. Some spectra are presented for measurements of the breakup of ^{24}Mg into ^{12}C + ^{12}C.

1. Introduction

Information from the study of nuclear reactions has expanded considerably during the last decade for both gamma ray and charged particle experiments, owing to the ability of experimentalists to observe events with high multiplicity. This development has resulted not only from the construction of larger arrays of detectors, but also from increasing the number of channels of electronics and the speed of multiparameter data acquisition systems. Compression in the size of electronics, and a downward trend in cost per channel has assisted this progress, whilst developments in the construction of larger semiconductor detectors such as large volume hyperpure germanium and large area ion-implanted silicon wafers have meant higher detection efficiencies.

In their review of cluster breakup of light nuclei, Fulton and Rae [1] describe how the use of inverse kinematics produces a forward focusing of the ejectiles in the experiment. Coincident detection of the two breakup particles enables the reconstruction of the relative energy, E_{rel}, between the breakup fragments from which the excitation energy, E_x, of the cluster states is determined. The resolution in E_{rel} and E_x was shown to be dominated by the angular (i.e. position) resolution obtained in the experiment.

In the work of Bennett et al. [2], Freer et al. [3], and Fulton et al. [4], an array of six detector telescopes was used, each telescope comprising three position sensitive silicon detectors with sensitive areas of about 10 mm × 10 mm and placed at 120 mm from the target. A thin (30 μm) ΔE front detector was used with a thicker middle detector to identify

* Corresponding author Tel +44 (21) 414 4680, fax +44 (21) 414 4719, e-mail: nmc@np.ph.bham.ac uk

[1] Present address Dept. of Physics and Astronomy, Schuster Laboratory, University of Manchester, Manchester, M13 9PL , UK.

[2] Present address: Dept. of Chemistry, University of Alabama at Huntsville, Huntsville, AL 35899, USA.

[3] Permanent address: Shanghai Institute of Nuclear Research, PO Box 800-204, Shanghai, China

SSDI 0168-9002(94)00874-4

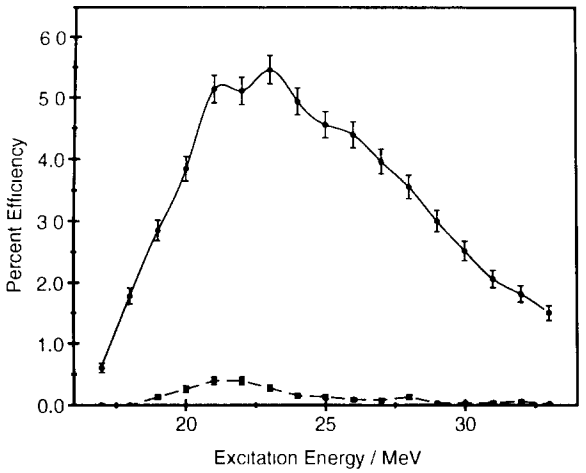

Fig. 1. Monte Carlo calculations of relative efficiency for coincident detection of breakup fragments from the $^{12}C(^{24}Mg,^{12}C\ ^{12}C)^{12}C$ reaction with E_{beam} = 170 MeV. Two detectors are centred at 14° and 14°, each 10 mm × 10 mm at 120 mm from the target (dashed line) and 50 mm × 50 mm at 240 mm from the target (solid line)

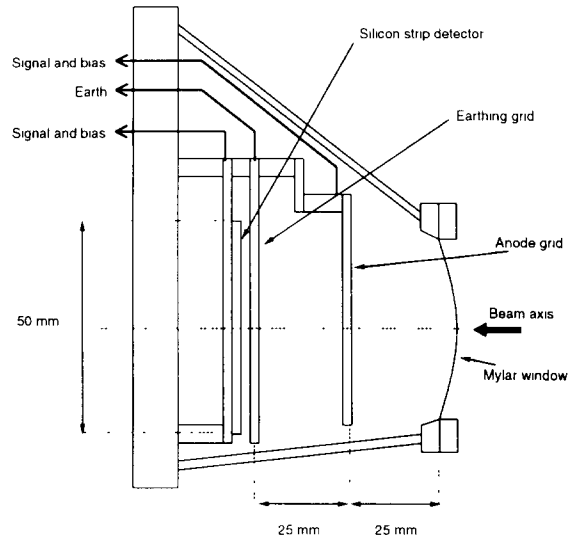

Fig. 2. Schematic diagram of the gas-silicon hybrid detector

the charge of the ions, and determine their energy, whilst the third detector was used to reject alpha particles. It was found that the ΔE detectors showed increasing leakage currents as radiation damage increased with time, and sometimes were unusable after a single experiment. The cost of regular replacement of these detectors places a major constraint on the size of any detector array.

To increase the detector efficiency for such breakup reactions, a design was developed to take advantage of newly available, large area, position sensitive silicon detectors with sixteen individual strips each 3 mm by 50 mm and placed 240 mm from the target. This design increases the solid angle, diminishes the dead space between detectors, and improves the angular resolution. A further advantage of strip detectors is that events with high multiplicity may be detected since each strip acts as an independent detector. Fig. 1 shows the results of "Monte Carlo" simulations of the coincident detector efficiency for the breakup reaction $^{12}C(^{24}Mg,^{12}C\ ^{12}C)^{12}C$ at 170 MeV. The efficiency profiles for a pair of 10 mm × 10 mm detectors at 120 mm (dashed line) is compared with that for a pair of 50 mm × 50 mm detectors placed at 240 mm from the target (solid line).

The larger distance from the target also reduces the radiation damage per unit area. However, detectors as thin as 30 μm or less cannot be made from large area silicon wafers, and the experimental programme demanded the detection of ions with masses 12–40 for which ΔE detectors with thicknesses equivalent to a few μm of Si were required. A gas filled ionization chamber was therefore chosen for the ΔE detector, based on existing designs which had been explored at the Nuclear Structure Facility, Daresbury Laboratory [5].

2. Construction of the hybrid detector

Fig. 2 shows a cutaway diagram of the complete hybrid detector. The detector box is constructed in stainless steel in three sections. The backplate is machined from solid material 10 mm thick and accommodates all the electrical and gas connections. The backplate carries an "O" ring in a groove to seal against the flange on the main body of the detector. This main body is made by folding and welding 2 mm sheets of stainless plate, and welding 5 mm stainless steel flanges at either end. The front of the detector is sealed by a gas-tight window held on a 5 mm frame.

The gas detector is an axial field ion chamber with a central gridded anode, operated with a continuous flow of isobutane or propane to maintain a typical internal pressure of 50–150 torr. The gas supply is monitored by a commercially available electronic valve and feedback system [5].

The ion chamber grids are constructed on standard printed circuit board (PCB) approximately 45 mm × 45 mm. The grid wires run perpendicular to the scattering plane, using 100 μm diameter beryllium copper wires spaced at 1 mm intervals, and orthogonal to the resistive strips in the silicon detector. The anode grid sits in the middle of the gas volume, 25 mm behind the front window and 25 mm in front of an optional second earthed grid which is 3 mm in front of the Si detector. The front window measuring 40 mm × 40 mm which encloses the gas volume is made from aluminized Mylar with thicknesses ranging from 1.5 to 6 μm, glued to the window frame and clamped against an "O" ring seal in the detector body. The aluminized side of the Mylar faces the gas volume and is separately earthed to the detector body. The high voltage for the anode is supplied through an external preamplifier via a "Conhex" connector on the rear flange. The ion chamber is operated at 2.5 V per torr cm.

The silicon detectors were custom made by Micron Semiconductor. Each is constructed as sixteen independent resistive strips 50 mm long and 3 mm high on a single substrate. Depletion depths from 300 to 1000 μm have been used. A common positive supply (typically 150 V) was provided to the rear (low resistance) detector face, via a simple decoupling network with two 10 nF capacitors and two 100 kΩ resistors.

The separate strips have a resistance of $\sim$3 kΩ and run horizontally in the detectors. The sum of the signals from each end measures the energy deposited by the incident ion, whilst the difference between the two signals divided by the sum is proportional to the position of the ionizing event. Each strip is independent, so events with high multiplicity can be recorded and the detector can be operated at much higher data rates before electronic pile-up becomes a problem. The overall count rate is limited by the gas filled ion chamber to about 10 kHz.

The Si detector carries a standard ribbon cable plug with a 34 way ribbon cable to a 34 pin feedthrough fixed into the rear detector flange using epoxy resin adhesive. Outside the detector box, the ribbon cable is passed through a box containing an adaptor circuit which provides a direct path for the leakage currents (via a 100 kΩ resistor) and presents an "offset" resistor in series between each end of a resistive strip and the virtual earth of the preamplifier. This resistor produces an offset in the charge division seen by the preamplifiers, and ensures that events occurring near the end of a strip produce large enough signals to pass over the threshold levels set on the analogue to digital convertors (ADCs) in the data acquisition system. The resistors are provided by standard plug-in resistor packs and the offset values are normally in the range 470 Ω–2 kΩ.

3. Electronics and data acquisition system

The Charissa electronics and data acquisition system was developed by the collaboration and originally installed at the Nuclear Structure Facility, Daresbury. It has now been transferred to the Department of Nuclear Physics at the Australian National University, Canberra, Australia.

A block diagram of the analogue and digital electronics is shown in Fig. 3. Charge pulses from the detectors are amplified by preamplifiers of Oxford design [6] with a sensitivity of 10 mV/MeV (Si) or 100 mV/MeV (Gas). The preamplifiers have a decay time constant of 50 μs, and may be fed with a test pulse generated by the rate divider circuit (Fig. 3 lower left) connected to the output of the Brookhaven Current Integrator.

The main shaping amplifiers use 1.5 μs time constants; the bipolar pulses are sent to the individual channels of ten 8-channel Silena analogue to digital converters (ADC) which have a common gate (see Fig. 3, right) generated by the master STROBE signal, 5 μs long.

The STROBE signal is generated by the logic system shown in the centre of Fig. 3. The exact layout may vary with different experiments or detector systems, that shown is appropriate for a system where two individual hybrid detectors are used to detect coincident events. Each amplifier generates a fast negative logic signal from the leading edge of the pulse, enabling fast decisions to be made in hardware.

For experiments where two coincident events are required (one from each detector), the logic signals are ORed in a Fan-In–Fan-Out (FIFO), and then form the STOP signals for the time to digital converters (TDCs). In experiments where events with higher multiplicity are required in each detector (such as the simultaneous detection of two alpha particles from ^{8}Be), individual logic signals are taken to one of six 8-channel LeCroy TDC modules.

For each hybrid detector a coincidence is formed between the logic from the gas detector and from the ORed logic from the Si strip detector. A rate divider then scales down the singles events by a factor of $1/n$ (in the range of 1/1 to 1/999) of the incident rate in order to sample the singles events for setting gains and software windows for particle identification. A master coincidence (Fig. 3, left of centre) between the telescope-1 and telescope-2 logic signals is then fed to the strobe-in FIFO, where it is ORed with singles triggers and those from the pulser system rate divider (Fig. 3, centre). The output STROBE initiates the whole sequence of the event acquisition, as well as providing a gate (TDC WINDOW) (1 μs) and the START signal for the TDCs (Fig. 3, right).

In cases where high multiplicity events are required for a valid event, the coincidence module can be replaced by a multiplicity unit; the choice of multiplicity to generate the STROBE signal is made by the front panel setting on the multiplicity unit.

Overall operation of the data acquisition is controlled by the Event Controller (EC), a purpose built CAMAC unit. This monitors the readout of the ADCs and TDCs as well as any other CAMAC devices incorporated into the system, such as pattern registers and scalers, and communicates with the computer event manager EM4 (Fig. 3, lower right).

The ADC conversion is complete in 32 μs, and the ADCs are then read out sequentially across a FERA highway into a cache memory store. The EC then examines the trigger link panel where the user indicates by means of a short patch cable which channels (corresponding to experimental parameters) are to be included in the event in addition to the ADCs, such as TDCs or other CAMAC channels. The "header word" for the event is then constructed and sent to a Read and Store Module (RSM), which constructs the event in memory by storing the "header" and "hit" words (corresponding to non-zero parameters) followed by the data words taken from the cache memory or the CAMAC devices. After approximately 90 μs the cycle is complete and then may be repeated.

The RSM continues to store event by event data in memory until a preset high water mark is passed, indicating the memory is nearly full; this causes the RSM to raise a Look

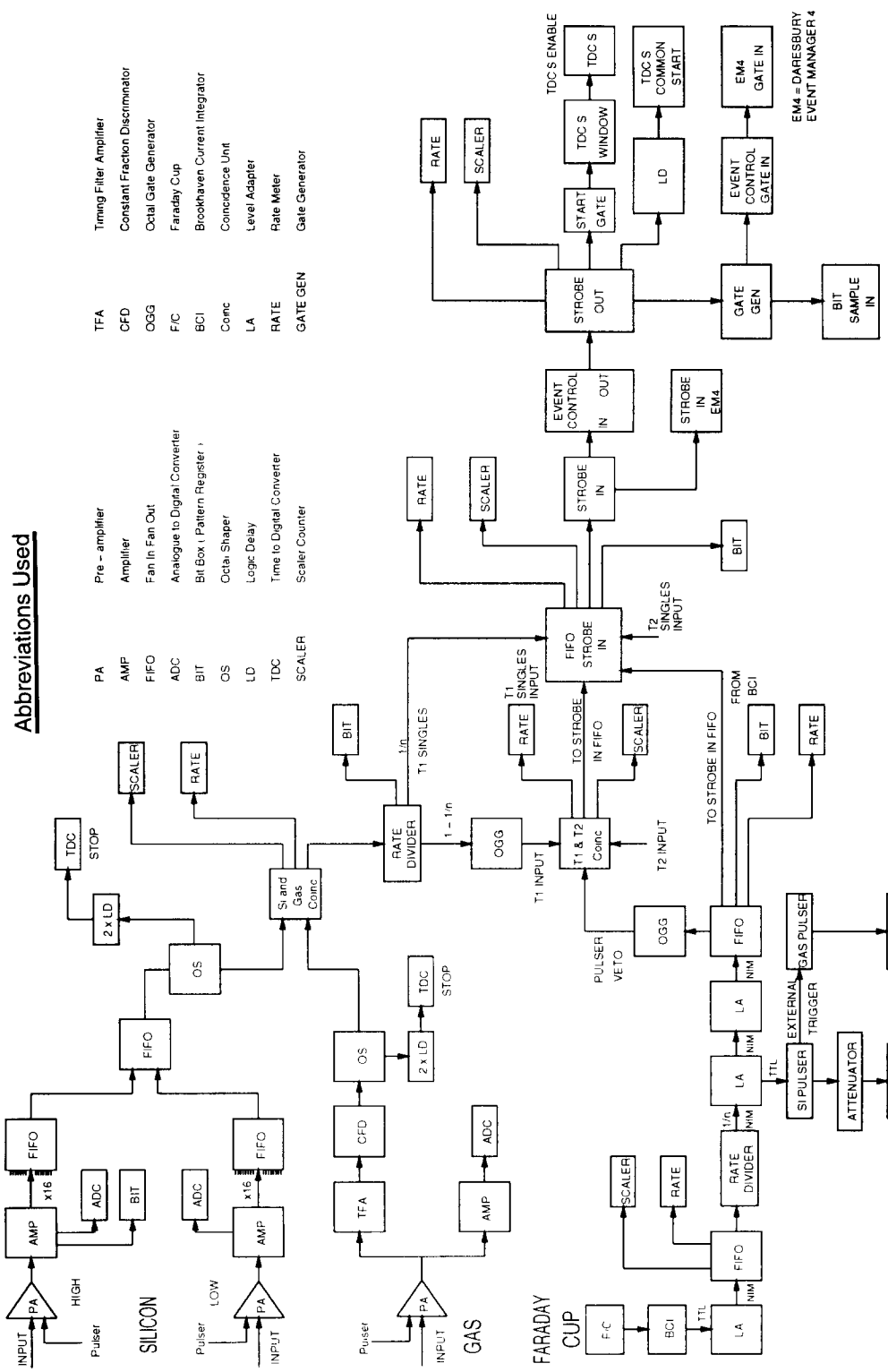

Fig. 3. Block diagram of the data acquisition electronics.

At Me (LAM) flag which forces the CAMAC serial crate controller to read the data from the RSM memory and pass it onto the computer where it is written to "Exabyte" tape cassettes.

At the end of each run, a number of on-line spectra are stored on disc as well as the values of CAMAC scalers which hold the information about the integrated beam current and numbers of single and coincidence events in each detector.

4. Experimental details and calibrations

A typical experimental setup might consist of two to four hybrid detectors placed at 240 mm from a target in the scattering chamber. Each detector is normally mounted on a separate arm. Thirty-two "Conhex" connectors are provided for each arm and carry the output signals from the adaptor boxes to exterior patch panels and the preamplifiers.

For calibration purposes a set of precision machined masks are fixed on mounts in front of the detectors; the angles of the slits in the masks are then calibrated using a telescope sighted along the beamline. The vacuum chamber is evacuated using the special gas handling and pumping set; this ensures that the chamber and the detector boxes are pumped simultaneously so that the delicate detector windows are never subjected to excessive differential pressure.

The accelerator beams are delivered to the target via a collimator tube containing spark machined tantalum apertures of 4 mm × 4 mm square situated 225 mm from the target and a 6 mm × 6 mm antiscatter aperture at 75 mm from the target. In experiments 95% of an 85 MeV ^{12}C beam would pass through a 1.5 mm × 1.5 mm tantalum aperture at the target position.

A precision pulser is used to set the amplifier gains so that there is good matching between both ends of each Si strip and between different Si strips. The first calibration runs are carried out without any gas in the detector. The elastic scattering of various ion species off a ^{197}Au target ($100\ \mu g\,cm^{-2}$) is used to provide monoenergetic scattered ions for the energy calibration, whilst scattering of the same ions from a ^{12}C target ($400\ \mu g\,cm^{-2}$) is used to provide a range of different energies to correct for ADC offsets. The scattering is repeated for each ion species corresponding to the breakup fragments to be detected. These calibrations are then repeated with the detector filled with gas at the correct pressure for running.

Once the calibration runs are complete, the vacuum chamber and detectors are refilled to atmospheric pressure with dry nitrogen, the masks are removed from in front of the detectors and the main running target is installed at the centre of the scattering chamber. After pumping the chamber to a suitable pressure, the principal beam is delivered to the chamber and the electronics are set to provide scaled-down singles data together with coincidence and pulser data using the beam and target for the main reaction of interest.

5. Performance of the detectors

5.1. Techniques for gain matching and removal of offsets

The data acquisition code provides all the features for viewing single and two- dimensional spectra, for installing software windows or gates, and for calculating and displaying calculated spectra using variable parameters in the computation. An on-line correction for the relative gain between ends of each strip can be made using the pulser peaks and altering the fine gain on the amplifiers, but is usually repeated off-line using the results of the elastic scattering.

When the data for the elastic scattering of ^{12}C off ^{197}Au are examined, a plot of energy versus position for any given resistive strip of the Si detector may look like Fig. 4a; the density of the dark areas is proportional to the number of counts so that the loci are simply an image of the slits in the mask across the detector face. The falloff in energy as a function of position across the face of the Si detector arises not simply from the kinematics of the scattering but also from a mismatch in the gains between the signals from the "low" angle (L) and "high" angle (H) ends of the strip detector. Applying a software gain factor g, the energy E and position P are now given by

$$E = Hg + L, \tag{1}$$

$$P = \frac{Hg - L}{Hg + L}, \tag{2}$$

resulting in the corrected spectrum shown in Fig. 4b with a gain factor of 1.092; the falloff in energy across the detector now results entirely from kinematics.

These equations assume good linearity of the preamplifier–amplifier–ADC chain; this has been tested using a precision pulser injected into the preamplifier and varying the pulser amplitude in fixed steps to produce a "matchsticks" spectrum. A weighted least squares fit to the centroids has confirmed excellent integral linearity (<0.05%) but shows some small offsets of about −0.2 to +0.2 V.

The ADC offsets can be observed by plotting the energy of scattered particles versus position along each strip, using data from a ^{12}C beam scattered from a ^{12}C target. These data contain a wide range of energies, allowing low energy ions to be seen; offsets in the ADC values at low pulse height values are seen as a curving of the energy versus position loci at low energies within the regions provided by the slits in the masks (Fig. 5a). To correct for this curvature an offset is added to the "low" and "high" ADC values before the energy and position are calculated. Eqs. (1) and (2) now become

$$E = (H + \mathrm{d}H)\,g + (L + \mathrm{d}L), \tag{3}$$

$$P = \frac{(H + \mathrm{d}H)\,g - (L + \mathrm{d}L)}{(H + \mathrm{d}H)\,g + (L + \mathrm{d}L)}. \tag{4}$$

It may be seen that the addition of offset corrections affects the gain factors and vice versa, so that an iterative pro-

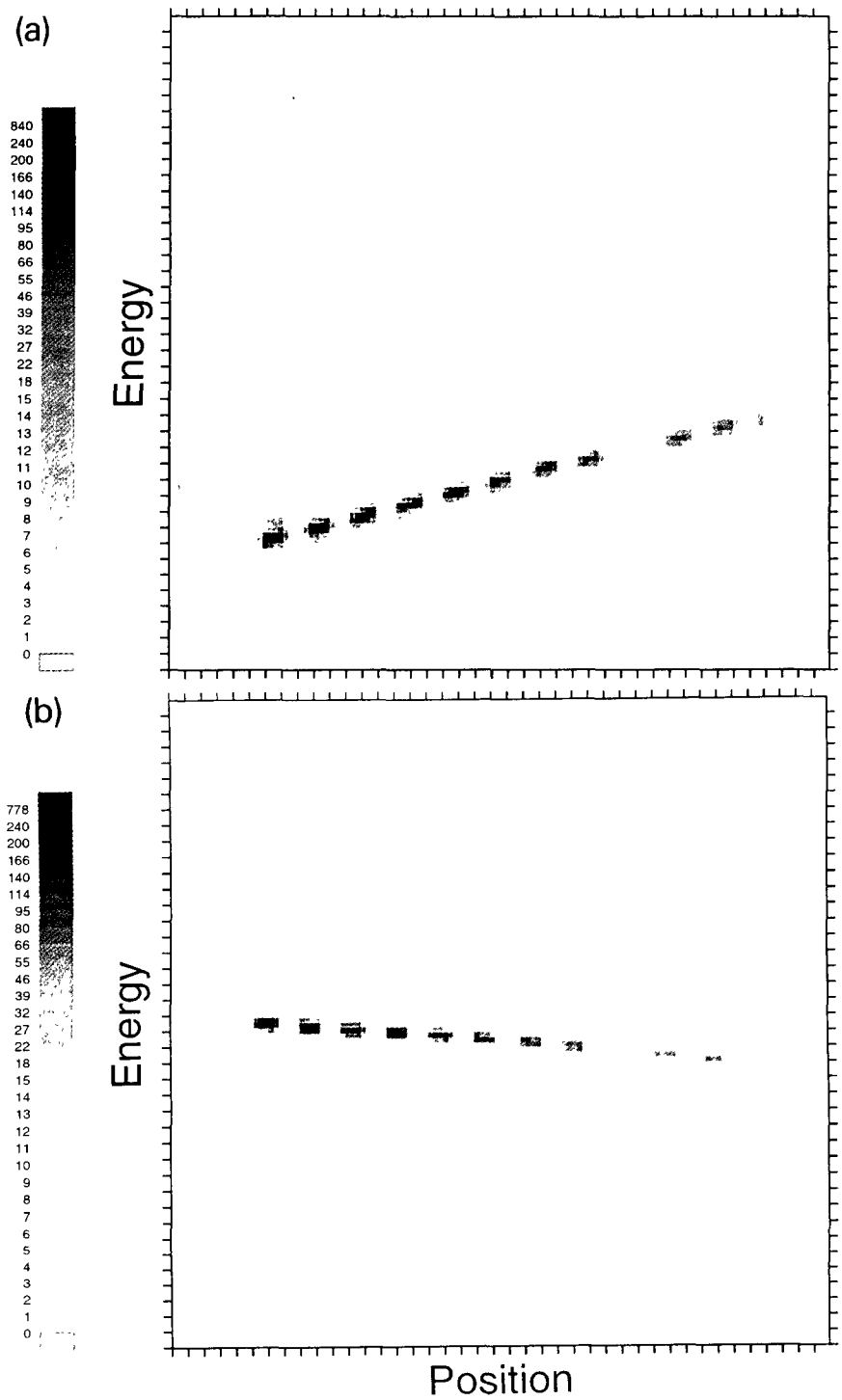

Fig 4. Two dimensional plots of the energy of ^{12}C elastically scattered from a ^{197}Au target versus position along a single silicon strip when a slitted mask is used in front of the detector; (a) uncorrected, (b) with software gain matching.

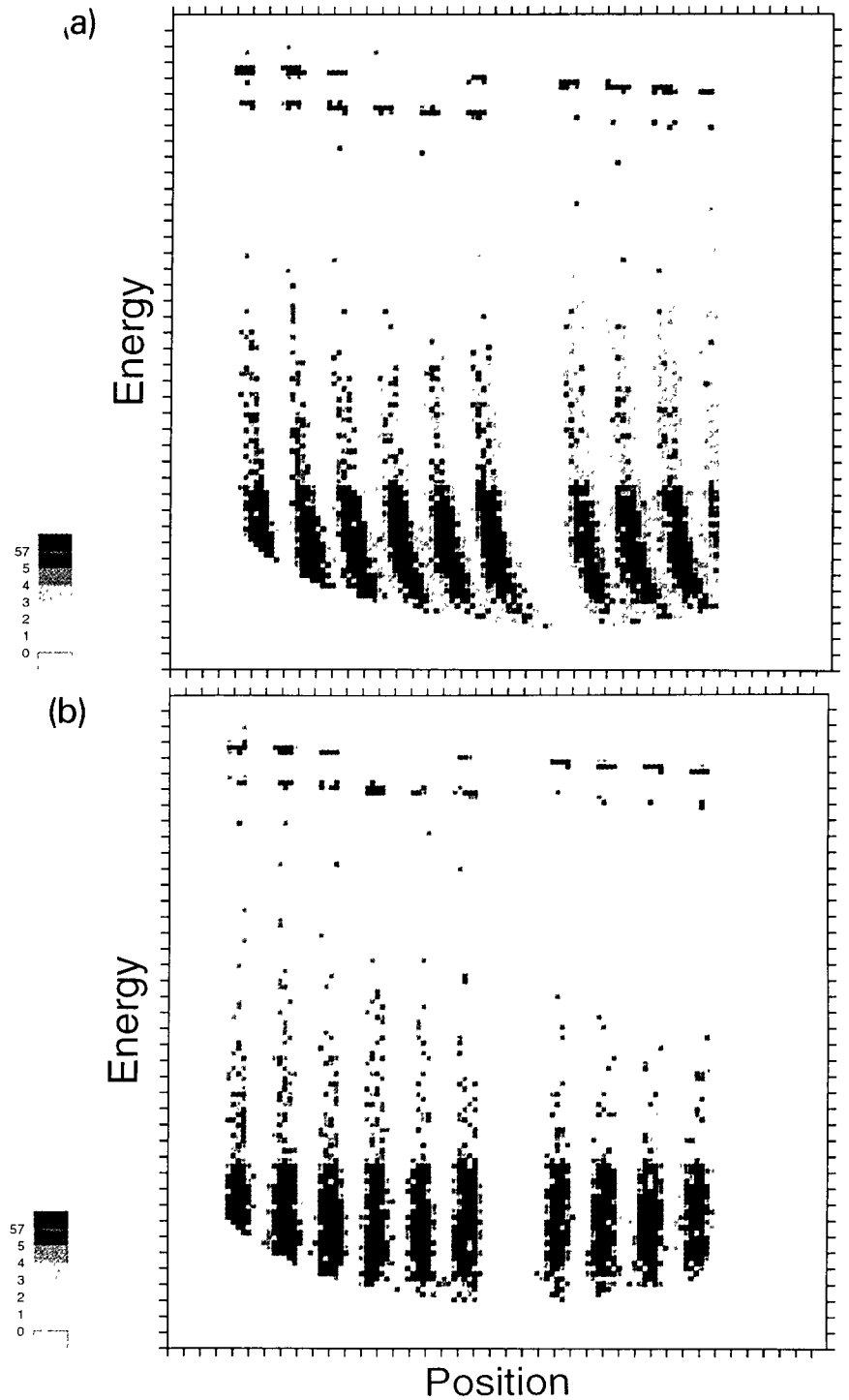

Fig. 5 Two dimensional plots of energy of ^{12}C ions scattered from a ^{12}C target versus position along a single strip when a slitted mask is used in front of the detector, (a) uncorrected with ADC offsets equal to 0, (b) corrected with offsets of -10 channels and $+14$ channels applied to the H and L ADC values respectively.

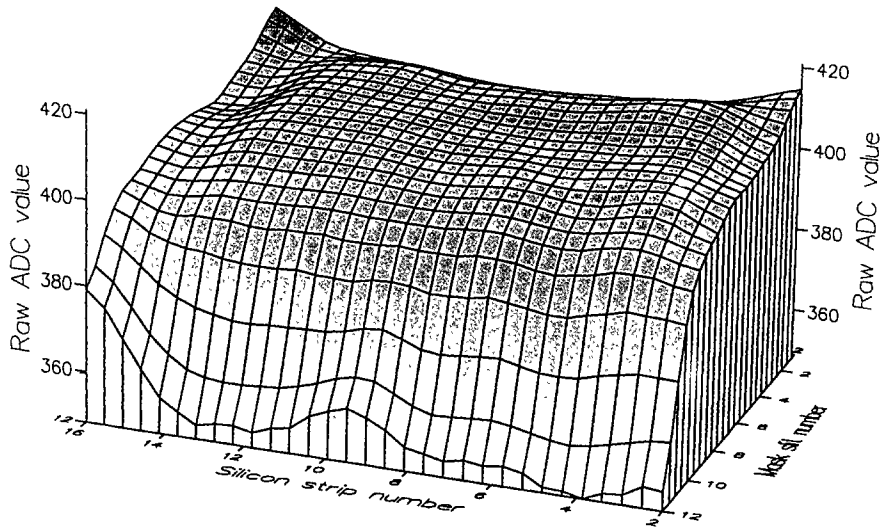

Fig 6 Variation of the gas detector signal as a function of position on the Si strip detector, for ^{12}C ions scattered from ^{197}Au at 90 MeV

cess of about three cycles is required to determine convergent values of gain and offset. A computer code now performs this automatially, and a typical result may be seen in Fig. 5b, using offset values of $dL = +14$, $dH = -10$ channels with L and H in the range 0–4096 channels. The gap in the spectrum (Fig. 5b) is caused by a missing slit in the masks which indicates the orientation of the detector with respect to the beam axis. Notice that some low energy events from the outermost mask slits now appear in the spectrum, since the offset corrections enable the events to pass through the software gates.

5.2. Response of the gas filled ion chamber

Fig. 6 shows a three dimensional plot of the pulse height spectrum for the gas filled ion chamber for ^{12}C ions scattered from ^{197}Au. This was constructed from the energy signals of the gas detector gated by software windows set on each of the silicon strips and on individual slits in the calibration masks. It shows a central region of almost uniform response, despite the "bowing" of the front window of the detector, with a pronounced fall off in pulse height towards the side of the detector where the body of the detector has a shallower slope, shown at the top in Fig. 2. Electrostatic modelling shows that the decline in pulse height for this side is expected because the detector body provides the earth plane for the anode grid. The energy loss signal from the gas is mapped as a function of position for each resistive strip to provide a polynomial correction factor for each strip. This correction represents the effective thickness of the gas volume and Mylar window at each position, and includes the effects of the bowing of the window due to the pressure differential.

5.3. Energy resolutions for the detector

Figs. 7 and 8 show respectively spectra from one of the Si strips and the gas detector for the elastic scattering of 84 MeV ^{12}C from ^{197}Au, and were obtained (after applying the corrections of Section 5.1), by placing software gates on the Si strip signals to confine events to a region 1.5 mm wide and 3 mm high. The gas detector yields a resolution with a FWHM of 650 keV, whilst the Si strip detector resolution achieves values of 205 keV FWHM without gas in the front section of the detector. Whilst the energy resolu-

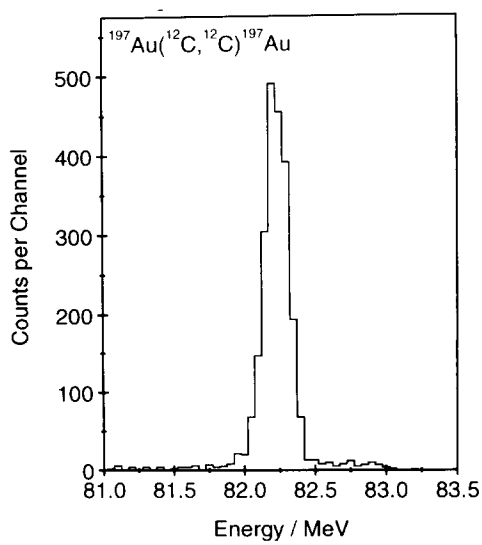

Fig 7 Energy spectrum obtained from a segment (1.5 mm wide by 3 mm high) of a single Si strip using elastic scattering of ^{12}C ions from a ^{197}Au target, indicating a FWHM of 205 keV

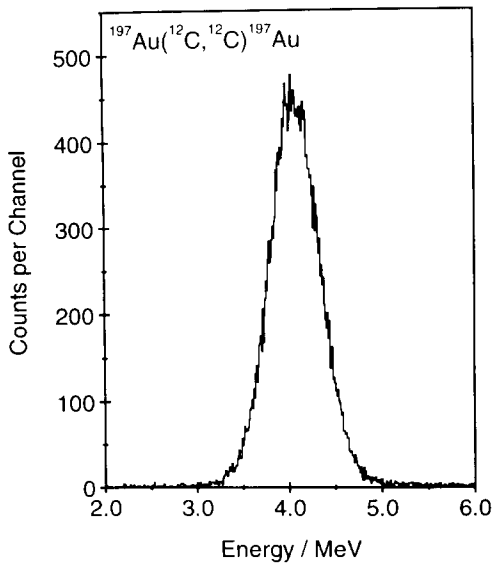

Fig. 8 Energy spectrum from the gas filled ion chamber corresponding to a single Si strip detecting ^{12}C ions scattered from a ^{197}Au target, indicating a FWHM of 650 keV.

tion of the gas portion of the detector is sufficient to achieve good particle identification (see Section 5.6), the addition of this signal to that from the Si strip detector produces a poor overall energy resolution. Our approach has been to identify the ions, and then use the Bethe–Bloch equation to calculate the mean energy loss in the gas, and then add this energy to that from the Si strip detector. The contribution to the resolution from the gas ΔE signal is then confined to the energy spread (straggling) in the gas. When the ion chamber is filled with gas, the resolution worsens in the Si strip detector to about 303 keV, implying an energy spread (straggling) of about 223 keV in the gas, assuming Gaussian distributions. For 85 MeV ^{12}C ions, and an energy loss in the gas of 4 MeV, this spread is calculated to be 181 keV (FWHM) [7], in reasonable agreement with this value.

5.4. Position resolution of the Si strip detectors

The calibration spectra using the ^{197}Au target are used to extract the final position spectrum for each mask slit, incorporating the changes in ADC gain and offset factors described in Section 5.1.

Fig. 9 shows an expanded position spectrum with a gas filled detector and the masks removed for elastic scattering of 170 MeV ^{24}Mg from ^{197}Au.

The main structure in this spectrum is caused by the "shadow" of the grid wires nearest to the Si detector and is consistent with the 1 mm spacing of the wires. This structure is modulated by the anode grid wires, the fringes overlapping every 10 wires. By measuring the FWTM (Full-Width-at-Tenth-Maximum) of the minima in this spectrum, an intrinsic resolution of 0.19 mm (FWHM) can be obtained which is unaffected by the presence (or absence) of the gas filling. In a coincidence experiment with two detectors, the overall efficiency is reduced to about 60% by the presence of the wires. Recent investigations using thinner, but more delicate, wires of 20 μm gold plated tungsten and with the shielding grid removed show no degradation of the detector performance, and resulted in an overall coincidence efficiency of about 96%.

5.5. (ΔE–E) relative timing resolution

With all energy and position corrections complete, the energy calibrations can now be recalculated and the final

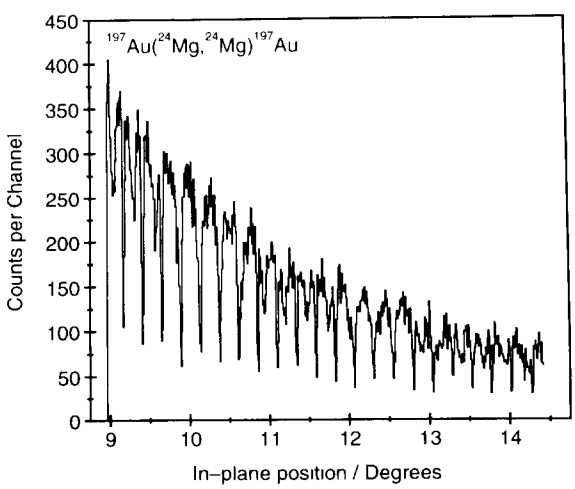

Fig. 9 Position spectrum from a single strip of the Si detector when the ion chamber is filled with gas for the scattering of ^{24}Mg ions from ^{197}Au

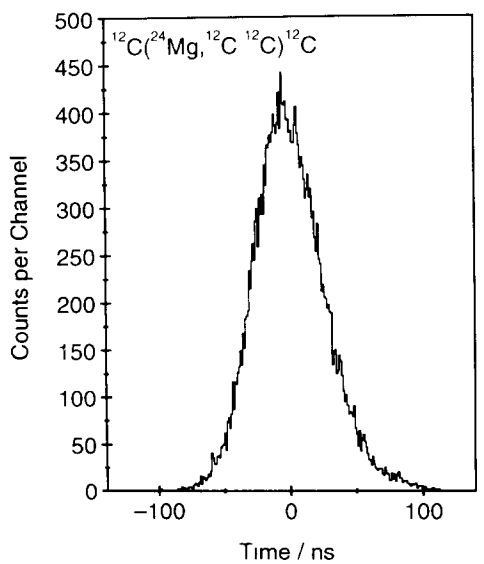

Fig. 10 Coincidence time spectrum calculated from the TDC values from all Si strips and the gas filled ion chamber, indicating a FWHM of 62 ns.

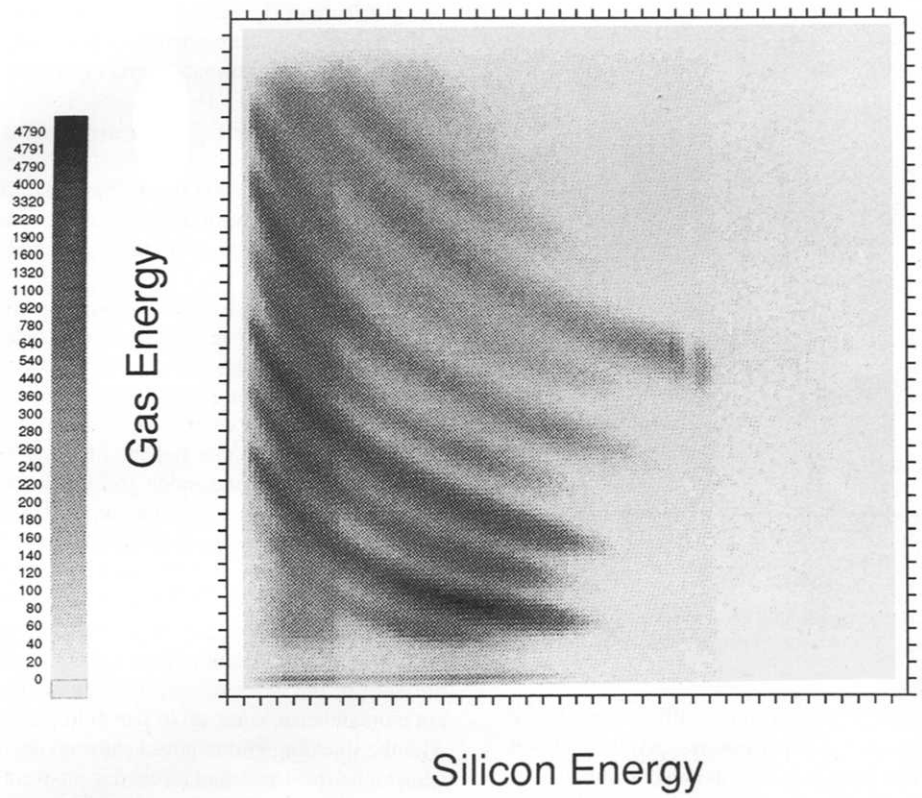

Fig 11. Particle identification spectrum obtained by plotting ΔE versus E for any given detector, and including all strips in the silicon detector

spectra sorted with specific dispersions in keV/channel, and with additional windows set on the spectra from the TDCs to ensure that events which fall outside certain time limits are not included. Fig. 10 shows a typical TDC spectrum of the time difference between the logic signals from the gas and Si detectors indicating a FWHM of 62 ns.

5.6. *Particle identification*

The energy (E) signals for the Si strip detectors can be combined with the signal ΔE from the gas detector to display two dimensional (2D) spectra to identify ions using the simplified Bethe–Bloch equation

$$\frac{\Delta E}{\mathrm{d}X} \propto \frac{MZ^2}{E}. \tag{5}$$

A plot of ΔE versus E for each hybrid detector therefore shows loci of constant MZ^2. Fig. 11 shows excellent identification of the ions from B to Si; the locus of Mg ions clearly shows a peak corresponding to elastic scattering from ^{12}C. Software windows or gates may be drawn around these loci to project out only those events which correspond to the ions of interest.

5.7. *Count rate limitations*

In recent runs at the Australian National University, the detectors have run at singles rates of 8–10 kHz, with the limit being set by pileup signals in the gas filled ion chamber.

6. Use of the detectors in breakup experiments

Once the ions have been identified and the energy (E) and position (P) signals obtained using the sort code, one can reconstruct the kinematics of the event. The hybrid detectors described in this work have been mostly used for the study of three body breakup reactions

$$\begin{aligned} \mathrm{A} + \mathrm{B} &\rightarrow \mathrm{C}^* + \mathrm{C}_3 \\ &\downarrow \\ \mathrm{C}^* &\rightarrow \mathrm{C}_1 + \mathrm{C}_2 . \end{aligned}$$

Fig. 12 shows a relative velocity diagram for the breakup fragments. The values of the positions $\boldsymbol{P}_1$, $\boldsymbol{P}_2$ from the two detectors allows calculation of the angles (θ_1 and θ_2) between the velocity vectors and the beam axis for the ejectiles C_1, C_2, and hence their momentum vectors $\boldsymbol{p}_1$ and $\boldsymbol{p}_2$, assuming correct mass identification for m_1 and m_2. The

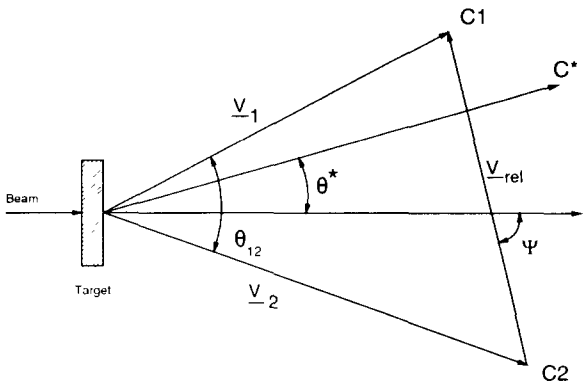

Fig 12 Relative velocity diagram for the breakup fragments

momentum p_3 of the undetected recoil particle C_3 can be calculated from

$$p_3 = p_{beam} - p_1 - p_2 \tag{6}$$

and hence E_3 calculated, since m_3 is now known, as a 3-body final state has been assumed. Since C_1 and C_2 are not necessarily coplanar with the beam axis, the angle θ_{12} between C_1 and C_2 is obtained from

$$p_1 \cdot p_2 = |p_1||p_2| \cos(\theta_{12}) . \tag{7}$$

The three body Q-value for the reaction can be found from

$$Q_3 = (E_1 + E_2 + E_3) - E_{beam} \tag{8}$$

and a spectrum incremented for the total energy

$$E_{tot} = E_1 + E_2 + E_3 = E_{beam} + Q_3 . \tag{9}$$

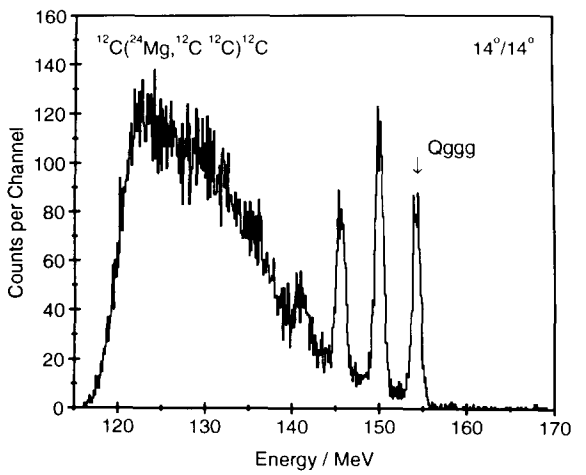

Fig. 13. Spectrum for the total fragment energy, E_{tot}, obtained for the breakup reaction $^{12}C(^{24}Mg,^{12}C\ ^{12}C)^{12}C$ with E_{beam} = 170 MeV

A typical E_{tot} spectrum (after offline corrections) is shown in Fig. 13 for the reaction $^{12}C(^{24}Mg,^{12}C\ ^{12}C)^{12}C$. The peak labelled Q_{ggg} corresponds to all three ejectiles in their ground states, whilst the two peaks at lower energy correspond to one and two ^{12}C ejectiles in their first excited states respectively. At higher excitation (lower energy) a broad continuum is seen corresponding to three-body breakup reactions which eject two ^{12}C particles and high excitation energy in the residual ^{12}C, or to four (or more)-body reactions.

By gating on the Q_{ggg} peak, a spectrum may be obtained for the relative kinetic energy E_{rel} of the breakup fragments in the rest frame of the parent nucleus. The relative velocity of the two fragments is given by

$$v_{rel}^2 = v_1^2 + v_2^2 - 2|v_1||v_2| \cos(\theta_{12}) . \tag{10}$$

using

$$E_{rel} = \tfrac{1}{2}\mu v_{rel}^2 , \tag{11}$$

where μ is the reduced mass of the breakup fragments

$$\mu = m_1 m_2 / (m_1 + m_2) , \tag{12}$$

we obtain

$$E_{rel} = \frac{1}{m_1 + m_2} \times \left[m_1 E_2 + m_2 E_1 - 2\sqrt{m_1 m_2 E_1 E_2} \cos\theta_{12}\right] . \tag{13}$$

The excitation energy in the nucleus C* is given by

$$E_x = E_{rel} - Q_2 , \tag{14}$$

where Q_2 is the two body Q-value for $C^* \rightarrow C_1 + C_2$

The structure in the E_{rel} spectrum may be difficult to see until all the off-line corrections have been completed.

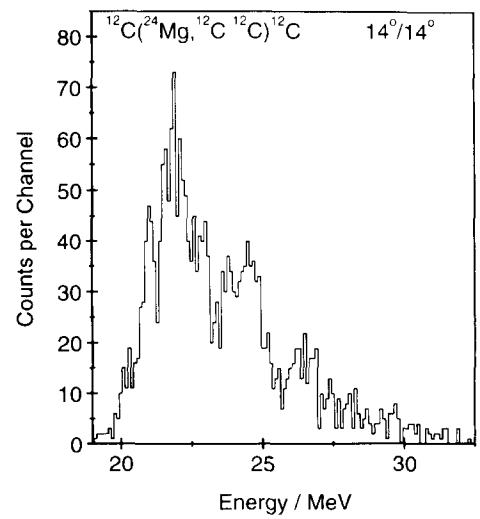

Fig. 14. An excitation energy spectrum for the breakup of ^{24}Mg into ^{12}C + ^{12}C using two detectors positioned at 14°/14°.

Fig. 14 shows the E_x spectrum after all corrections have been carried out. The dominant contribution to the energy resolution in this spectrum should come from the position (angular) resolution of detectors as detailed in Bennett [8]. Using our figures of 0.19 mm and 200 keV (FWHM) for the Si detector would suggest contributions to the value of of E_{rel} about 5 keV from each of these sources for a symmetric event. However, Monte Carlo simulations suggest contributions nearer to 30 keV when more asymmetric events are included, and indicate that multiple scattering in the target may be the dominant contribution to the overall resolution of the excitation spectrum which is measured to be about 150 keV FWHM for a typical experiment.

7. Summary

A hybrid detector has been constructed using a new design of Si strip detector within a gridded gas filled ionization chamber. The Si detector is of large area (50 mm $\times$ 50 mm) with sixteen resistive strips which yield both energy and position signals and enable events with high multiplicity to be detected. Energy resolutions of 200 keV (FWHM) and position resolutions approaching 0.19 mm (FWHM) have been obtained for 84 MeV ^{12}C ions scattered from a 100 $\mu g\,cm^{-2}$ ^{197}Au target. The gas part of the detector gives an energy resolution of about 650 keV (FWHM) for the same elastic scattering, a time resolution of about 60 ns (FWHM) in coincidence with the Si detector and is capable of resolving ions up to $Z = 20$. However, there is some loss of detector efficiency from the grid wires in the ion chamber, and in current experiments the 100 μm wires have been replaced by 20 μm gold plated tungsten wires. Once all the off line corrections have been carried out, the excitation energy spectra from breakup events can be reconstructed with intrinsic resolutions of about 150 keV.

Acknowledgements

The authors would like to acknowledge the skills and efforts of the technical staff at the Nuclear Structure Facility, Daresbury, during the development of the detector. The authors would also like to thank the staff and students of the Department of Nuclear Physics, Australian National University for their help and encouragement during the relocation of the Charissa experimental programme. The authors acknowledge the Science and Engineering Research Council for research grants to the institutions involved in this work and SERC research studentships for NC, ASt.JM, JSP, SMS, SPC, SPF, CDJ and PMS, and a CASE studentship for MJL.

References

[1] B.R. Fulton and W.D.M. Rae, J. Phys. G 16 (1990) 333.
[2] S.J. Bennett, M. Freer, B.R. Fulton, J.T. Murgatroyd, P.J. Woods, S.C. Allcock, W.D.M. Rae, A.E. Smith, J.S. Lilley and R.R. Betts, Nucl. Phys. A 534 (1991) 445.
[3] M. Freer, S.J. Bennett, B.R. Fulton, J.T. Murgatroyd, G.J. Gyapong, N.S. Jarvis, C.D. Jones, D.L. Watson, J.D. Brown, R.A. Hunt, W.D.M. Rae, A.E. Smith and J.S. Lilley, in: Interaction of nuclear structure and heavy ion dynamics, Institute of Physics Conference series 109 (1990) p. 243.
[4] B.R. Fulton, S.J. Bennett, M. Freer, J.T. Murgatroyd, G.J. Gyapong, N.S. Jarvis, C.D. Jones, D.L. Watson, J.D. Brown, W.D.M. Rae, A.E. Smith and J.S. Lilley, Phys. Rev. Lett. B 267 (1991) 325
[5] R.A. Cunningham, N.E. Sanderson, W.N.J. Snodgrass, D.W. Banes, S.D. Hoath and J.N. Mo, Nucl. Instr. and Meth. A 234 (1985) 67, A.E. Smith, Appendix to Daresbury Annual Report Nucl. Phys. (1990/91) p. 115.
[6] P.J.S. Bromley-Barratt, Charissa preamplifier design (unpublished)
[7] N.M. Clarke, Nucl. Instr. and Meth. 96 (1971) 497
[8] S.J. Bennett, N.M. Clarke, M. Freer, B.R. Fulton, S.J. Hall, O. Karban, J.T. Murgatroyd, G. Tungate, G.J. Gyapong, N.S. Jarvis, D.L.Watson, W.D.M. Rae, A.E. Smith, J.S. Lilley, P.J. Woods and R.D. Page, Nucl. Instr. and Meth. A 332 (1993) 476.